AAS 11 - 511

# Design and Implementation of the ARTEMIS Lunar Transfer Using Multi-body Dynamics

David Folta*, Mark Woodard†
Theodore Sweetser‡, Stephen B. Broschart‡,
and
Daniel Cosgrove§

**Abstract**

The use of multi-body dynamics to design the transfer of spacecraft from Earth elliptical orbits to the Earth-Moon libration ($L_1$ and $L_2$) orbits has been successfully demonstrated by the Acceleration Reconnection and Turbulence and Electrodynamics of the Moon's Interaction with the Sun (ARTEMIS) mission. Operational support of the two ARTEMIS spacecraft is a final step in the realization of a design process that can be used to transfer spacecraft with restrictive operational constraints and fuel limitations. The focus of this paper is to describe in detail the processes and implementation of this successful approach.

## INTRODUCTION

The use of multi-body dynamics to design the transfer of spacecraft from Earth elliptical orbits to the Earth-Moon libration ($L_1$ and $L_2$) orbits via Sun-Earth weak stability regions has been successfully demonstrated by the Acceleration Reconnection and Turbulence and Electrodynamics of the Moon's Interaction with the Sun (ARTEMIS) mission. This flight of the two ARTEMIS spacecraft is a final step in the realization of a design process that can be used to transfer spacecraft with restrictive operational constraints and fuel limitations.

Design methods incorporating multi-body dynamics were applied with optimization of numerically integrated states. The integration uses high fidelity models with objectives of trajectory conditions near various manifold structures that are combined to ensure the design was successful given inherent modeling, navigation, and maneuver execution errors. The ARTEMIS design involves two distinct transfers using the Sun-Earth libration ($L_1$ and $L_2$) regions and demonstrates their potential.[1,2,3,4,5] The design incorporates lunar gravity assists, of which one was a double gravity assist with a 13-day interval between lunar encounters, to achieve the required energy and orbital orientation to place the spacecraft on the appropriate transfer manifold. We then exploit the flow direction consistent with a Lissajous trajectory manifold to attain the final Earth-Moon libration conditions. Operational support then focused on maintaining the desired manifold structure or hopping onto a nearby manifold which

* Aerospace Engineer, NASA Goddard Space Flight Center, Building 11, Room S116, Greenbelt, Maryland 20771. Senior Member AIAA.
† Aerospace Engineer, NASA Goddard Space Flight Center, Building 11, Room C001, Greenbelt, Maryland 20771. Member AIAA
‡ Mission Design Engineer,. Jet Propulsion Laboratory, California Institute of Technology, Pasadena, CA 91100
‡‡ Mission Design Engineer,. Jet Propulsion Laboratory, California Institute of Technology, Pasadena, CA 91100
§ Flight Dynamics Lead, University of California at Berkeley / Space Sciences Lab, 7 Gauss Way #7450, Berkeley, CA 94720

yield similar end conditions as the flow shifts from dynamically stable to unstable modes. The implementation considered operational constraints, navigation errors and un-modeled perturbations.

To compute maneuver requirements in terms of Delta-velocity ($\Delta v$), our strategy involves various numerical methods: traditional Differential Corrections (DC) targeting with central or forward differencing and SQP-based optimization using the VF13AD algorithm from the Harwell library. The DC generates a-priori conditions, is used in the optimization sequence, and is used for verification of $\Delta v$ magnitudes and directions. For the DC, equality constraints are incorporated, while for optimization, nonlinear equality and inequality constraints are employed. These constraints incorporate both the desired target conditions at the Earth-Moon system as well as the spacecraft constraints on the $\Delta v$ direction and relationship between the spin axis and the $\Delta v$ vector. The end goal of the transfer phase was to achieve the Earth-Moon Lissajous insertion conditions necessary for a minimal energy insertion into the Earth-Moon $L_2$ (EM $L_2$) or $L_1$ (EM $L_1$) Lissajous orbits. These goals were held constant over the stable manifold of the mission design process but were allowed to vary upon the final trajectory that crossed from Sun-Earth unstable manifold onto the Earth-Moon stable manifold. Along the transfer maneuvers were executed, each adjusting the trajectory slightly to converge to the chosen target. These designs are very sensitive to mis-modeled perturbations and to the maneuver errors. The paper addresses the lunar gravity assists, the optimization techniques as well as numerical solutions, sensitivity of the transfer, correction maneuvers, manifolds, and the trajectory design implemented. We also describe the processes and implementation of this successful approach.

**ARTEMIS Mission Background**

The ARTEMIS mission was approved in May 2008 as an extension to the Time History of Events and Macroscale Interactions during Substorms (THEMIS) mission.[1] THEMIS encompasses five spacecraft in Earth orbit. The ARTEMIS mission utilized two spacecraft in the outer-most elliptical Earth orbits and, with lunar gravity assists, re-directing the spacecraft to both the $L_1$ and $L_2$ Earth-Moon libration point orbits via transfer trajectories that exploit the multi-body dynamical environment. The two spacecraft are denoted as P1 for the THEMIS B spacecraft and P2 for the THEMIS C spacecraft. The THEMIS team had long known that substantial orbit maneuvers would be necessary for the P1 and P2 spacecraft to avoid entering a deep umbra shadow that would drain all power from the batteries and put the spacecraft into a non-recoverable power state. At the request of the Principal Investigator (PI), analysts at the Jet Propulsion Laboratory (JPL) provided a concept for a transfer trajectory for both P1 and P2. The maneuver plan included a series a propulsive Orbit-Raising Maneuvers (ORMs) to position each spacecraft for a series of lunar and Earth gravity assist maneuvers. The injections onto the transfer orbits for P1 and P2 occurred in February and March 2010 with the targeted multiple lunar flybys. The P1 spacecraft entered the EM $L_2$ Lissajous orbit on August 25, 2010 and the P2 spacecraft followed on October 22, 2010. On June 27$^{th}$ and July 17$^{th}$ of 2011, both spacecraft transferred into highly elliptical lunar orbits. The original design for the P1 and P2 transfers are shown in Figures 1 and 2. ARTEMIS uses simultaneous measurements of particles and electric and magnetic fields from two locations to provide the first three-dimensional information on how energetic particle acceleration occurs near the Moon's orbit, in the distant magnetosphere, and in the solar wind. ARTEMIS has collected unprecedented observations of the refilling of the space environment behind the dark side of the Moon by the solar wind.

**Trajectory Design Background**

The exploitation of multi-body dynamical environments to permit the transfer of spacecraft from Earth to Sun-Earth weak stability regions and then return to the EM $L_1$ and EM $L_2$orbits has been successfully accomplished.[5] This demonstrated transfer is a positive step in the realization of a design process that can be used to transfer spacecraft with minimal $\Delta v$ expenditure. Initialized using gravity assists to overcome fuel constraints; the ARTEMIS mission design has successfully placed two

spacecraft into Earth-Moon libration orbits by means of this application of forces from multiple gravity fields.

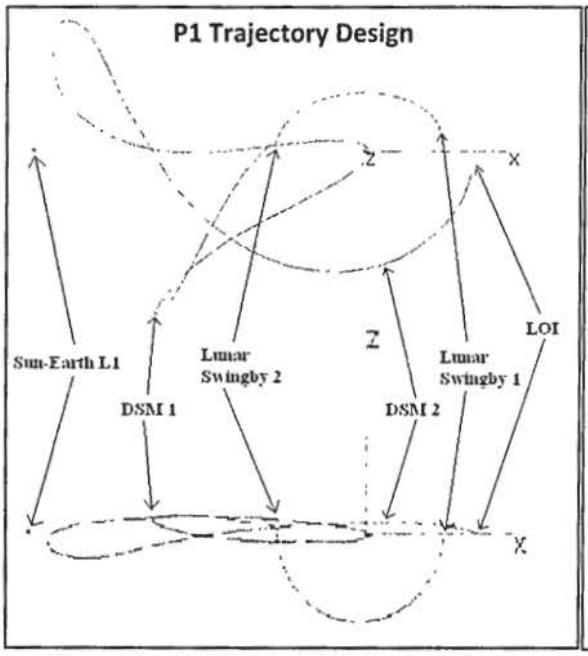


**Figure 1. P1 Original Trajectory Design (Top view is X-Y projection, Bottom is X-Z)**

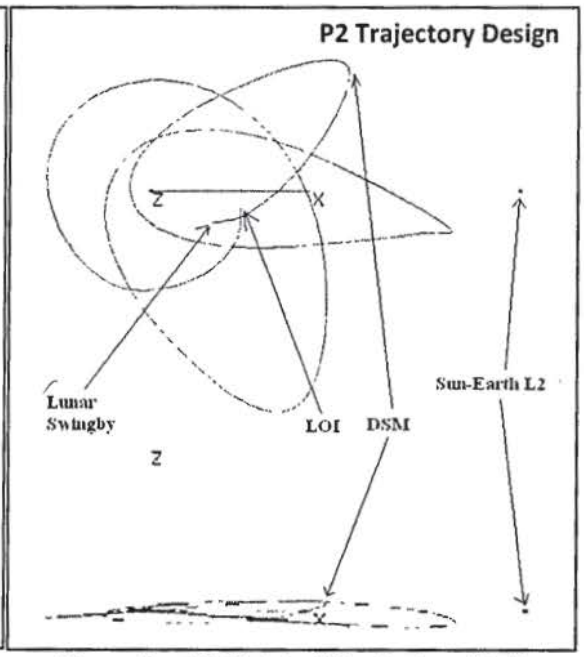


**Figure 2. P2 Original Trajectory Design (Top view is X-Y projection, Bottom is X-Z)**

Various design methods relying on multi-body dynamics were applied to achieve these transfers.[6-17] Generation of manifolds from dynamical information, optimization of forward numerically integrated states, and the selection of various trajectory conditions near various manifold structures were combined to ensure the design was successful given inherent modeling, navigation, and maneuver execution errors. The ARTEMIS design involved two distinct transfers, one for each spacecraft, which demonstrates the potential in the application. The design incorporated lunar gravity assists (one of which used a double gravity assist with a 13-day interval between lunar encounters), to achieve the correct energy and orbital orientation to place the vehicles on the appropriate transfer arc. Having placed the spacecraft onto trajectories which can exploit the flow direction consistent with a Lissajous trajectory manifold to attain the final Earth-Moon orbital conditions, operational support then focused on remaining near a manifold structure, given navigation errors and mismodeled perturbations as the flow shifts from dynamically stable to unstable modes.

Along this transfer trajectory, several maneuvers were executed, each adjusting the trajectory slightly, each converging to the chosen target of an Earth-Moon libration orbit insertion location at the desired epoch. These designs are very sensitive to mismodeled perturbations and to the maneuver errors. The paper addresses the lunar gravity assists, manifold generation, the optimization techniques as well as numerical solutions, sensitivity of the transfer, and the operational navigation solutions, and trajectory design implemented.

As a final multi-body mission goal, ARTEMIS is the first spacecraft to navigate to and perform stationkeeping operations around the EM $L_1$ and EM $L_2$ Lagrangian points. The NASA Goddard Space Flight Center (GSFC) has previous mission experience flying in the Sun-Earth $L_1$ (SOHO, ACE, WIND, ISEE-3) and $L_2$ regimes (WMAP, ISEE-3) and have maintained these spacecraft in libration point orbits by performing regular orbit stationkeeping maneuvers. The ARTEMIS mission was built on these

experiences, but stationkeeping in Earth-Moon libration orbits presented new challenges since the libration point orbit period is on the order of two weeks rather than six months. As a result, stationkeeping maneuvers to maintain the Lissajous orbit were performed weekly, and the orbit determination solutions between maneuvers were required to be quite accurate.

### ARTEMIS Spacecraft Overview

Each ARTEMIS spacecraft is spin-stabilized with a nominal spin rate of roughly 20 RPM. Spacecraft attitude and rate are determined using telemetry from a Sun sensor (SS), a three-axis magnetometer (TAM) used near Earth perigee, and two single-axis inertial rate units (IRUs). The propulsion system on each spacecraft is a simple monopropellant hydrazine blow-down system. The propellant is stored in two equally-sized tanks and either tank can supply propellant to any of the thrusters through a series of latch valves. Each observatory was launched with a dry mass of 77 kg and 49 kg of propellant, supplying a wet mass of 126 kg at beginning of life.

Each spacecraft has four 4.4 Newton (N) thrusters – two axial thrusters and two tangential thrusters. The two tangential thrusters are mounted on one side of the spacecraft and the two axial thrusters are mounted on the lower deck, as seen in Figure 3. The thrusters fire singly or in pairs – in continuous or pulsed mode – to provide orbit, attitude, and spin rate control. Orbit maneuvers can be implemented by firing the axial thrusters in continuous mode, the tangential thrusters in pulsed mode, or a combination of the two (beta mode). Since there are no thrusters on the upper deck, the combined thrust vector is constrained to the lower hemisphere of the spacecraft.

### ARTEMIS Spacecraft Maneuvers Constraints

The ARTEMIS spacecraft are spinning vehicles with the spin axis pointed within 5 degrees of the south ecliptic pole. These spacecraft can implement a $\Delta v$ (thrust direction) along the spin axis towards the south ecliptic pole direction or in the spin plane, but cannot produce a $\Delta v$ in the northern hemisphere relative to the ecliptic. While the axial thrusters can be used if necessary, these thrusters are not calibrated as well as the radial thrusters. This constraint limited the location of maneuvers and these maneuvers were performed in a radial direction. For the lunar gravity assist and the multi-body dynamical environment, the trajectory was optimized using a nonlinear constraint that placed the $\Delta v$ in the spin plane. The maneuver epoch was also varied to yield an optimal radial maneuver magnitude.

In addition to the direction of maneuvers, another 'error' source also resulted in some interesting maneuver planning. This is the fact that, as a spinning spacecraft, a maneuver was quantized into ~ 2 cm/s intervals with a start time that is dependent upon the Sun pulse in each spin. This meant that there was a finite maneuver accuracy that could be achieved that was dependent upon the $\Delta v$ magnitude for each maneuver. Some maneuvers could be quantized by varying the maneuver epoch, but DSN coverage often led to this method not being easily enacted. Thus many maneuvers are taken with the associated errors from spin pulse and timing.

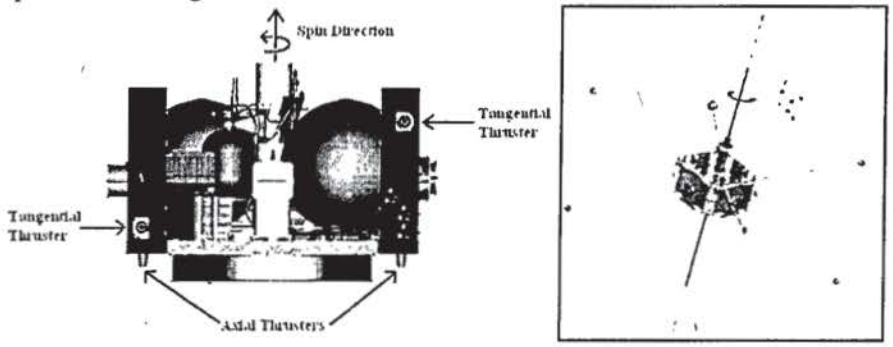


**Figure 3. ARTEMIS Spacecraft Bus Design**

## TRANSFER TRAJECTORY DESIGN

The original ARTEMIS trajectory designs are illustrated in Figures 1 and 2. The two diagrams show the ARTEMIS P1 and P2 trajectories in the Sun-Earth rotating frame during the translunar phase. These general designs were originally determined using dynamical processes with software tools called LTOOL and MYSTIC.[17] During the pre-mission concept phase, these tools provided for the inclusion of the multi-body environment and optimization techniques combine with general manifold knowledge of previous research.[refs] The challenge was to compute a viable transfer that permitted correct outgoing energy and asymptote directions that could be achieved by lunar gravity assist. To achieve the gravity assist, Orbit-Raising Maneuvers (ORMs) were required near periapsis to methodically raise apoapsis to lunar distance. The ORMs are carefully timed to phase the final apoapsis approach with lunar approach to achieve a lunar gravity assist maneuver. Gravity assists are a key component of the ARTEMIS trajectory design, as neither spacecraft has sufficient propellant to perform a direct insertion into the Earth-Moon libration point orbits. During the last few orbits prior to the lunar encounter, small Lunar Targeting Maneuvers (LTMs) and Trajectory Correction Maneuvers (TCMs) corrected for maneuver execution errors during the last ORMs and align the lunar approach trajectory to the proper B-plane targets.

### Multi-Body Dynamical Environment Phase

Following the first close lunar gravity assist, the P1 spacecraft flew under the Earth and performed a second gravity assist roughly 13 days later, as seen in the Sun-Earth rotating frame in Figure 2. A Deep Space Maneuver (DSM1) was performed 33 days later. DSM1 targeted through Earth periapsis and to the Earth-Moon libration insertion state. Following the Earth periapsis, the P1 spacecraft once again transferred into the general vicinity of the Sun-Earth $L_1$ Lagrangian point. This region is also identified as a "weak stability boundary" region. At the final bend in the P1 trajectory, the spacecraft was at a maximum range of 1.50 million km from the Earth. At this point, the trajectory began to fall back towards the Earth-Moon system on an unstable Lissajous manifold. A second deep space maneuver (DSM2) to target the EM $L_2$ Lagrangian point was originally planned but not required. A small maneuver was performed to insert P1 into the proper $L_2$ Lissajous orbit. The P2 translunar trajectory used a single lunar swingby and three deep space maneuvers, two Earth periapses, and the Lissajous orbit insertion maneuver.

For both P1 and P2, we allocated 4% of the total propellant budget to perform any required trajectory correction maneuvers (TCMs) along the way. The trajectory design focused on achieving the Earth-Moon libration insertion conditions to achieve a Lissajous orbit and which would permit the final stage of the ARTEMIS mission, a transfer to a highly eccentric lunar orbit. Following the lunar flyby targeting phase that included several flybys at ranges from 50,000km to just over 11,000km, the transfer trajectory began. The flyby targets were required to enable the energy to place the ARTEMIS spacecraft near the appropriate outgoing manifolds. Since the two spacecraft were originally designed for a different mission - a highly elliptical Earth orbit - and were already flying, fuel was (and is) extremely limited. Thus, with the unique operational constraints, accomplishing the transfer goals with the minimum fuel cost was the highest priority, allowing the designs to take very indirect paths to the final targets.

### Perturbation Model Fidelity

A full ephemeris model (DE405 file) was used which incorporated point mass gravity representing Earth, Moon, Sun, Jupiter, Saturn, Venus, and Mars. Also included was an eighth degree and order Earth potential model. The solar radiation pressure force was based on the measured spacecraft area and the estimated mass (from bookkeeping) and the coefficient of reflectivity from navigation estimation. The trajectory simulations are based on a variable step Runge-Kutta 8/9 and Prince-Dormand 8/9 integrator. The libration point locations are also calculated instantaneously at the same integration interval. Initial

conditions used thoughtout the maneuver planning process correspond to the UCB delivered navigation solutions using both the DSN and the UCB tracking system. While several coordinates systems are used, the baseline ARTEMIS mission specified Earth Centered Cartesian (TOD) coordinates and an Earth-Moon rotating system. Software tools used in this process include the General Mission Analysis Tool (GMAT) developed at GSFC as an open source high fidelity tool with optimization and MATLAB® connectivity and the Analytical Graphics Inc (AGI) STK/Astrogator suite.

**Optimization of Maneuvers**

To compute maneuver requirements in terms of ΔV, our strategy involved various numerical methods: traditional Differential Corrections (DC) targeting with central or forward differencing and optimization using the VF13AD algorithm from the Harwell library. A DC process provided for an a-priori condition, within the optimization process, and is also used for verification of the Δv magnitude and direction. For the DC, equality constraints were incorporated, while for optimization, nonlinear equality and inequality constraints were employed. These constraints incorporated both the desired target conditions at the Earth-Moon system as well as the spacecraft constraints on the Δv direction and relationship between the spin axis and the Δv vector. To target to the desired Earth-Moon Lissajous conditions, we incorporated several variables and constraints which are representative control parameters for correction maneuvers. These values can vary by a factor of ten, depending on the sensitivity of the trajectory. The control variables are the Δv Cartesian components with perturbations set between 1e-8 to 1e-10 (m/s) and the maximum step-size permitted ranging from 1e-3 to 1e-5 (m/s). Sample P1 targeted states, epoch, and angle information with respect to the spin axis are shown in Tables 3 and 4.

**Navigation Uncertainties**

Throughout the entire trajectory design process, navigation solutions were generated at a regular frequency of once every day with the exception of post-maneuver navigation solutions which were made available once a converged solution was determined. The rapid response was to ensure that the maneuver had performed as predicted and that no unanticipated major changes to the design were necessary. Table 1 includes a list of the major navigation solutions used in maneuver planning and their uncertainties. As seen, the RSS of the uncertainties are on the order of 10's of meters in position and below 1 cm/s in velocity. As a conservative estimate for maneuver planning and error analysis, 1σ uncertainties of 1 km in position and 1 cm/s in velocity are used. These accuracies were obtained using nominal tracking arcs of one three-hour contact every other day. This frequency of contacts was investigated earlier in the mission design process and was thought to meet the accuracy goals as stated above. The Goddard Trajectory Determination System (GTDS) is used for all navigation estimation.

**Table 1. P1 and P2 Navigation Solution Uncertainties during Transfer Trajectory**

| Phase | Navigation Arc Length (days) | Position Accuracy (m) (1σ) | Velocity Accuracy (cm/s) (1σ) |
|---|---|---|---|
| P1 Lunar Assist 1 | 5 | 10 | 0.05 |
| P1 Lunar Assist 2 (post FB) | 2 | 1500 | 1.00 |
| P1 Deep Space | 21 | 34 | 0.09 |
| P1 TCM2 | 7 | 43 | 0.11 |
| P1 TCM5 | 7 | 43 | 0.11 |
| Pre P1 Lissajous Insertion | 7 | 0.2 | 0.01 |
| P2 Lunar Assist 1 | 3 | 30 | 0.01 |
| P2 Deep Space | 13 | 12 | 0.04 |
| P2 TCM1 | 10 | 51 | 0.02 |
| Pre P2 Lissajous Insertion | 7 | 0.7 | 0.05 |

## END-TO-END TRAJECTORY DESIGN

The transfer trajectory design approach uses both the numerical methods as discussed above with the inclusion of dynamical systems for verification and to gain knowledge of the transfer dynamics. The transfers were implemented as designed and, then, knowledge of the Sun-Earth/Moon dynamics was applied to verify that the target conditions would be met. The spacecraft were targeted to the libration point orbit insertion location knowing full well that maneuver execution and navigation errors would push the path off the 'baseline' design. A correction maneuver was planned that would essentially shift the trajectory, such that the new path would be consistent with a nearby manifold or the expected flow in this regime.

A forward integrating numerical optimization process fits well with respect to the spacecraft constraints for the purpose of calculating optimized $\Delta$vs. This optimization procedure permitted minimization of the $\Delta$v magnitude, variation of the $\Delta$v components in azimuth, as well as variation of the maneuver epoch, while incorporating the nonlinear constraint on the spacecraft $\Delta$v direction relative to the spin axis. The manifold computations supplied the intuitive design but could not be used effectively at this point to also constrain the maneuver directions. An example of two manifolds as applied to the ARTEMIS P1 trajectory design appears in Figure 4. The left plot represents the computation of stable manifolds progressing towards a Sun-Earth $L_1$ Lissajous trajectory and illustrates (in red) a local manifold originating at the post-DSM position along the path and arriving in the vicinity of the Sun-Earth $L_1$ Lissajous orbit. The figure (right side) reflects unstable manifolds that depart from the Sun-Earth $L_1$ Lissajous trajectory, illustrating a local manifold (in red) that flows towards the point along this Sun-Earth unstable manifold that reaches the EM $L_2$ Lissajous entry region, that is, it approaches the stable manifold associated with EM $L_2$ Lissajous trajectory. The trajectory design reflects the merger of these two local manifolds to complete the mission (that is, the unstable manifold from the Sun-Earth $L_1$ region to blend into the stable manifold that delivers the vehicle to the EM $L_2$ vicinity). For flow information to serve as a basis for the P2 transfer the stable manifolds associated with the EM $L_2$ Lissajous trajectory were propagated backwards and transformed directly to the Sun-Earth coordinate frame; the P2 path blended into the flow consistent the Earth-Moon manifolds directly from the relatively large DSM maneuver.

In reality, as the TCM maneuvers were performed, the path essentially jumped from the vicinity of one local manifold to another, at a slightly different energy level, to manage both the trajectory design and the mission constraints. The manifolds realized were generated using the initial condition (post-maneuver). To ensure that a verifiable trajectory solution was realized, the optimized maneuver solutions were correlated with these manifolds. The number of optimized maneuvers was very low and their magnitudes quite small, considering the sensitivity of the dynamics and uncertainties of the OD solutions.

### EM-Libration Insertion Targets

The end goal of the transfer phase was to achieve the Earth-Moon Lissajous insertion conditions necessary for a minimal energy insertion into the EM $L_1$ or EM $L_2$ Lissajous orbits. The goals were defined in terms of the Earth J2000 Coordinates and are shown in Tables 2 and 3. These targets were held constant over the entire mission design process. As part of the early design process, a minimum $\Delta$v was necessary since the bulk of the fuel had been used in the prime science mission. This left the designers with a fuel budget that could get them to the Moon directly, but without the required fuel to insert into lunar orbit. Although a baseline trajectory is defined to design the mission, there is no true reference motion that is required.

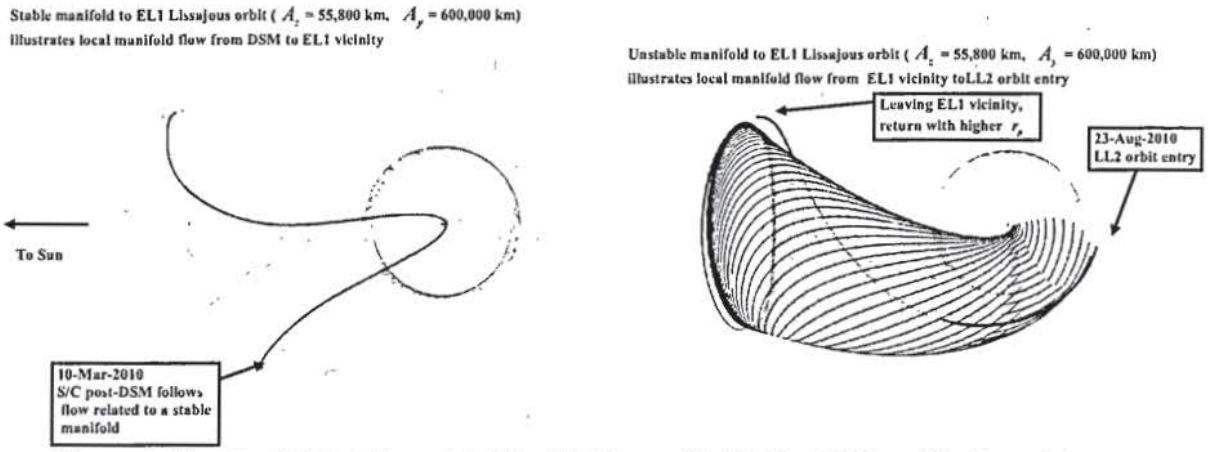


**Figure 4. Baseline P1 Out-Bound to Max Radius on Stable Manifold and In-Bound to Lissajous Orbit on Unstable Manifold**

**Table 2. Sample P1 Linear and Non-Linear Constraints**

| Target / Constraint | EM $L_2$ Goals (in Earth J2000 Coord) | Tolerance |
|---|---|---|
| X position | 352031 km | 1 km |
| Y position | -318469 km | 1 km |
| Z position | -131402 km | 1 km |
| Julian Date Epoch | 2455431.500 | 60 sec |
| Non-linear: Δv angle wrt Spin Axis | 89 deg | .05 deg |

**Table 3. Sample P2 Linear and Non-Linear Constraints**

| Target / Constraint | EM $L_2$ Goals (in Earth J2000 Coord) | Tolerance |
|---|---|---|
| X position | 352031 km | 1 km |
| Y position | -318469 km | 1 km |
| Z position | -131402 km | 1 km |
| Julian Date Epoch | 2455431.500 | 60 sec |
| Non-linear: Δv angle wrt Spin Axis | 89 deg | .05 deg |

### Trajectory Correction Maneuver Design and Placement

As the transfer trajectory was flown, correction maneuvers were required to adjust for maneuver execution errors of the previous maneuver, the spacecraft pointing errors, as well as the navigation errors. These maneuvers, called Trajectory Correction Maneuvers (TCM), represent the statistical maneuvers along the transfer. A deterministic maneuver included in both the P1 and P2 design was called a Deep Space Maneuver (DSM), to separate it from the maneuvers and correction maneuvers performed while in the elliptical orbit which raised the apoapsis and eventually targeted the lunar gravity assists. At each maneuver location, the optimizer was run to determine the minimal Δv location. To determine an a priori maneuver location and to achieve an intuitive feel for the maneuver results, a DC process was also performed which anticipated maneuver locations based on DSN coverage and how the

manifold behaved. Table 4 includes the P1 spacecraft maneuver information for all the post-DSM transfer trajectory maneuvers. In Table 5, the P2 spacecraft maneuver information is listed for all the transfer trajectory maneuvers. Note that P1 TCM numbers originate at '4', reflecting the corrections performed only in the multi-body dynamical environment phase. For P1, maneuvers TCM1 through TCM4 were completed in the elliptical orbit or during lunar gravity assist targeting, with the P1 TCM4 executed between the double lunar gravity assist. For P2 TCM1 & TCM2 were used as corrections to DSM1 and DSM2. Since thruster locations dictated that we could only perform maneuvers in the "down" direction, these TCMs were placed in optimal locations around the orbit to correct for the hot or cold maneuver execution performance of TCM1 and TCM2. As shown in Tables 4 and 5, the maneuver execution errors are small at only a few percent. These errors are a function of actual start time with respect to a Sun pulse of a spinning spacecraft, tank temperatures, attitude knowledge, and the general propulsion system performance.

**Table 4. P1 Trajectory Correction Maneuvers**

| Maneuver | Epoch (UTC) | Δv Magnitude (m/s) | Final Maneuver Error (%) | Reason for Maneuver |
|---|---|---|---|---|
| TCM 4 | January 31, 2010 @ 07:03 | 0.12 | 1.0 | Navigation errors |
| DSM | March 10, 2010 @ 19:00 | 7.30 | 1.46 | Deterministic Δv |
| TCM 5 | April 20, 2010 @ 09:00 | 0.18 | -2.06 | DSM Correction |
| TCM 6 | June 20, 2010 @ 21:45 | 0.18 | -3.24 | TCM 5 Correction |
| TCM 7 | July 19, 2010 @ 23:00 | 0.66 | 0.61 | Arrival Epoch |
| TCM 8 | August 18, 2010 @ 06:00 | 1.90 | n/a | Arrival Epoch |

**Table 5. P2 Trajectory Correction Maneuvers**

| Maneuver | Epoch (UTC) | Δv Magnitude (m/s) | Final Maneuver Error (%) | Reason for Maneuver |
|---|---|---|---|---|
| TCM 1 | March 26, 2010 @ 02:05 | 0.65 | -0.60 | Lunar Flyby Correction |
| DSM 1 | May 13, 2010 @ 02:21 | 3.68 | -3.43 | Deterministic Δv |
| DSM 2 | June 1, 2010 @ 14:50 | 24.25 | -0.57 | Deterministic Δv |
| TCM 2 | July 20, 2010 @ 12:00 | 2.22 | 0.28 | DSM 2 Correction |
| TCM 3 | August 2, 2010 @ 12:00 | 0.64 | 1.90 | DSM 2 Correction |
| DSM 3 | September 9, 2010 14:00 | 2.58 | n/a | Arrival Epoch and EM $L_1$ Z-Evolution |
| TCM4 | October 01, 2010 11:00 | 0.31 | n/a | DSM 3 Correction |
| TCM5 | October 12, 2010 13:40 | 0.26 | n/a | DSM 3 Correction |

Figures 5 and 6 show the locations of the P1 and P2 maneuvers and related information during the multi-body dynamical environment phase in each case. The maneuvers compensate for the maneuver execution errors, the navigation errors, and the subsequent maneuvers to correct for these errors. These errors and small mis-modeled perturbations can lead not only to late or early arrival times at the prescribed Lissajous insertion location, but also contribute to out-of-plane affects and may result in trajectories that intersect with the Moon. Clearly, the trajectory is very sensitive to such small perturbations. But, that sensitivity also implies that small corrections can alter the trajectory design significantly and allow fine control.

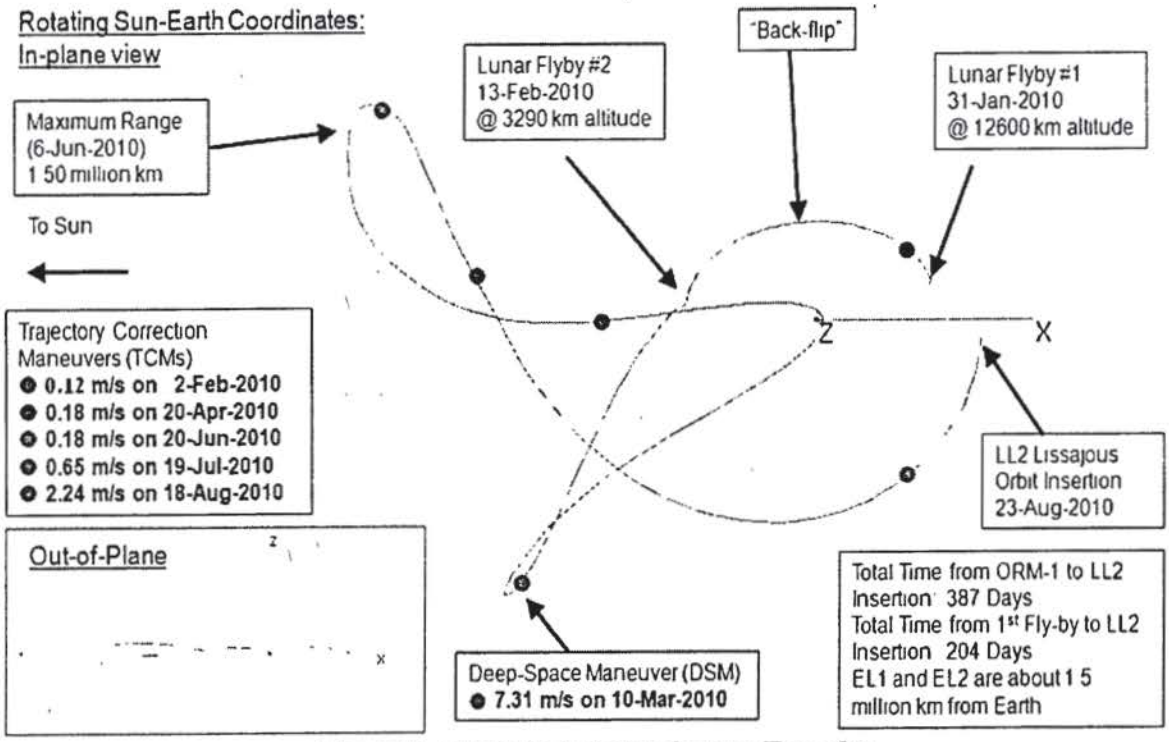


**Figure 5. P1 Multi-body Trajectory Transfer**

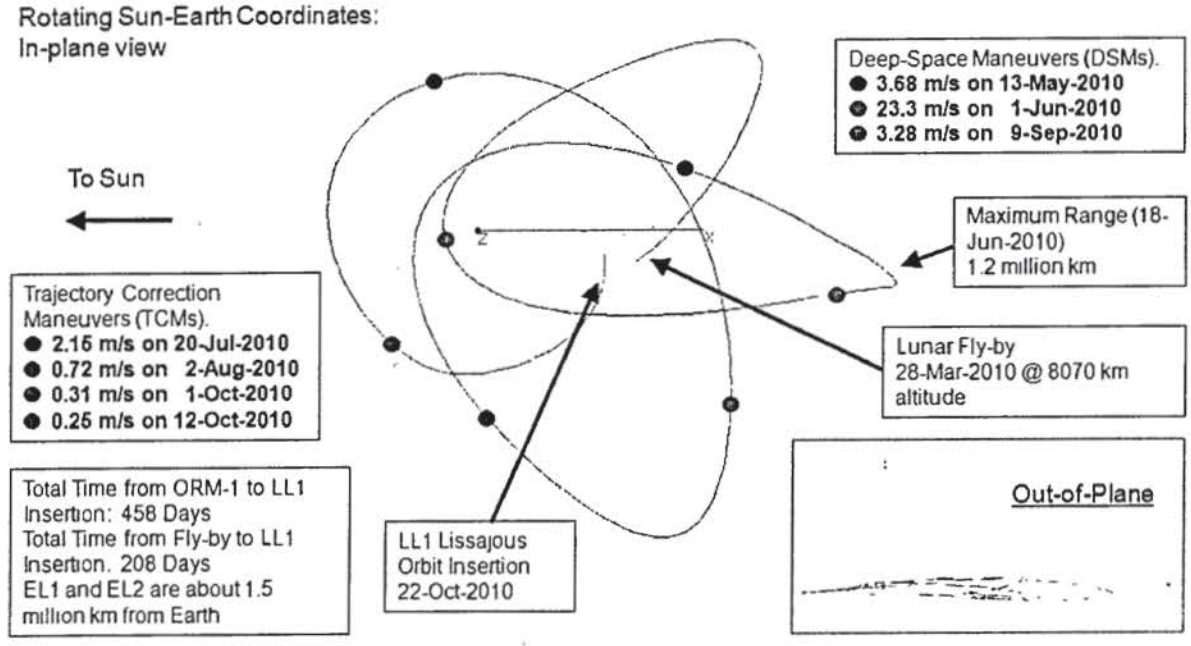


**Figure 6. P2 Multi-body Trajectory Transfer**

**Trajectory Correction Maneuver Analysis**

Trajectory Correction Maneuvers (TCMs) were analyzed for all phases of the transfer trajectory. In addition, knowing the general path of the stable and unstable manifolds provided us with insight as to the location of maneuvers to adjust the trajectory while meeting the axial constraints of the spacecraft (no 'up' maneuvers permitted). To ensure that the correction maneuver placement minimized the Δvs, a Monte Carlo (MC) analysis was also performed while using the optimization process to plan the operational maneuver. This allowed us to investigate the angle of the Δv with respect to the spacecraft spin plane as well as the ecliptic plane. In performing these analyses, one quickly finds locations on the Sun-Earth multi-body regions which permit the correct Δv direction. We also focused on trying to make each and every TCM a radial maneuver. The concern was that errors in ongoing or planned maneuver performance would result in a needed correction direction that could not be met. Below are examples of the Monte Carlo analysis for the TCMs during the mid part of the P1 double lunar gravity assist and both P1 and P2 transfers. The assumed errors in our MC analysis used a 1km and 1 cm/s navigation error along with 1% hot and cold maneuver performance. Attitude uncertainty was briefly used, but did not represent a large effect as compared to the navigation errors.

The pre gravity assist targets were analyzed and found that there were locations between the P1 lunar gravity assist that permitted a down maneuver to correct for any error in the targeted lunar B-Plane. Figures 7 through 12 show the results of the MC for this phase. Figure 7 shows the distribution of the second P1 flyby with anticipated navigation errors of 0.1 km and 0.1 cm/s after the first flyby occurs. It shows a large distribution in the B-plane. After achieving the first flyby on Jan 31st, 2010 with the B-plane within the require tolerance, an analysis was performed to determine if a TCM4 was needed. The MC for TCM4 Δv and the related B-plane errors after TCM4 are shown in Figures 8 and 9.

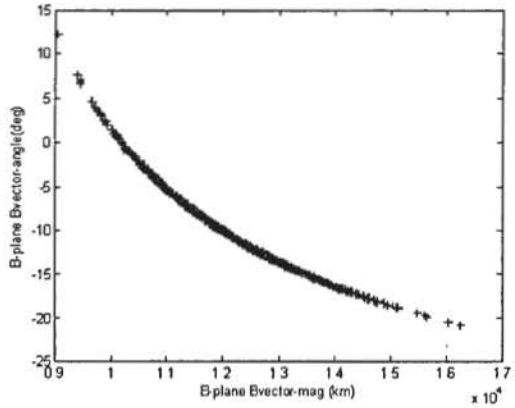


**Figure 7. 2nd Flyby B-Plane Distribution with Navigation errors**

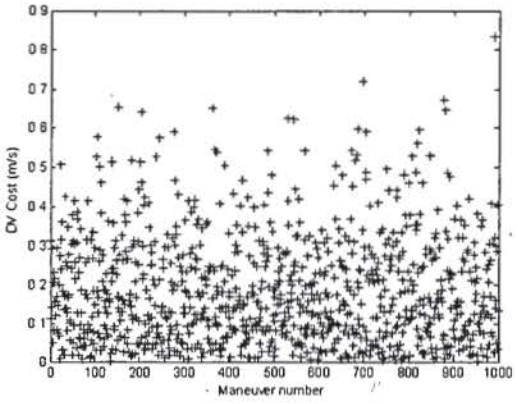


**Figure 8. TCM4 Δv corrections**

Once the first flyby was achieved, the TCM4 maneuver planning was completed for a TCM shortly after the first flyby. The anticipated errors on the second flyby after TCM4 were relatively small, at a standard deviation of 7.793 km in the B-magnitude and 0.05 deg in the B-angle.

After the second flyby for P1 and the only flyby for P2, MC analysis was completed to examine the effect of the Δv errors on deterministic maneuvers in the multi-body phase. A selection of maneuver epochs was chosen based on the tracking and contact schedule. We analyzed combined maneuvers with the DSM and an earlier TCM a few days after the second gravity assist, but optimization of the operational navigation solutions indicated that a DSM alone would suffice.

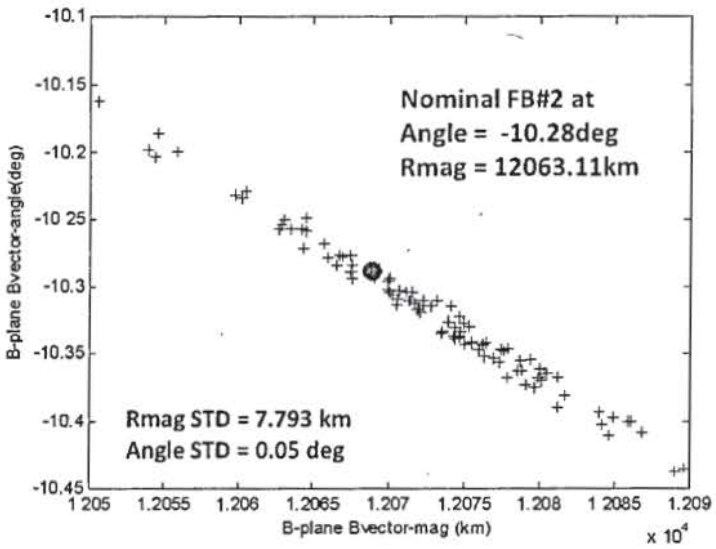


**Figure 9. Post TCM4 Estimated B-plane errors**

At this point in our analysis it was becoming obvious that to meet the libration orbit insertion Cartesian states, the Z-axis target component needed to be relaxed. In doing this, the incoming insertion epoch could also be adjusted to give a representative Earth-Moon Lissajous orbit that met the overall mission requirements for the final lunar inclination after the libration orbit phase was completed.

The DSM analysis centered on the minimization of the required Δv to arrive at the libration insertion parameters shown in Tables 2 and 3. The DSM epoch was varied to meet DSN contact schedules and to maintain a radial maneuver. During this post flyby analysis it was found that the achieved B-plane parameter was within 6 km of the desired target and well within the epoch for the flyby as shown in Table 6. At this point in the trajectory design process, a 'nominal' DSM plan was executed for a total Δv of 7.73 m/s. Once the DSM was computed, planning began on the TCMs to correct for both the DSM maneuver performance errors and the errors due to navigation and third body effects.

**Table 6. P1 B-Plane Components at Flyby #2 (Feb 15th)**

| OD Solution DOY | B-plane Magnitude | B-magnitude Error | B-plane Theta | B-plane Theta Error | Time of Perislene |
|---|---|---|---|---|---|
| nominal | 11931.048 | n/a | -11.734 | n/a | 09:54:34 |
| 33 | 11924.048 | -4.649 | -11.7038 | 0.0297 | 09:54:38 |
| 34 | 11926.399 | -4.666 | -11.7161 | 0.0174 | 09:54:38 |
| 35 | 11926.379 | -4.669 | -11.7168 | 0.0167 | 09:54:38 |
| 36 | 11926.368 | -4.679 | -11.7163 | 0.0172 | 09:54:38 |
| 37 | 11925.932 | -5.116 | -11.7158 | 0.0177 | 09:54:40 |
| 38 | 11925.815 | -5.233 | -11.7154 | 0.0181 | 09:54:40 |
| 39 | 11925.330 | -5.718 | -11.7148 | 0.0187 | 09:54:38 |

The TCM5 MC analysis to meet the libration insertion goals is show in Figure 10. A 100 case MC was run using just the Navigation errors with a radial maneuver fixed to a 90 degree angle. The results give a mean Δv of 0.201 m/s with a maximum of 0.675 m/s, and minimum of 0.004 m/s, and a median Δv of 0.171 m/s. As we processed the GMAN simulation of the planned TCMs, the libration insertion components varied significantly. For example a difference of +/- 1 pulse (~ 1.5 cm/s) in the maneuver

execution of 15 pulses yield a difference in the insertion Cartesian targets of 5000km in X, 1000 km in Y, and 500 km in Z. This sensitivity meant that combined with navigation uncertainties, we would have a TCM 6.

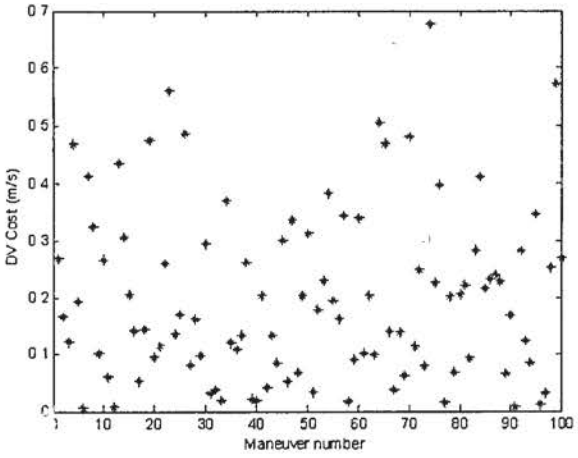


**Figure 10. P1 TCM5 Δv MC Analysis**

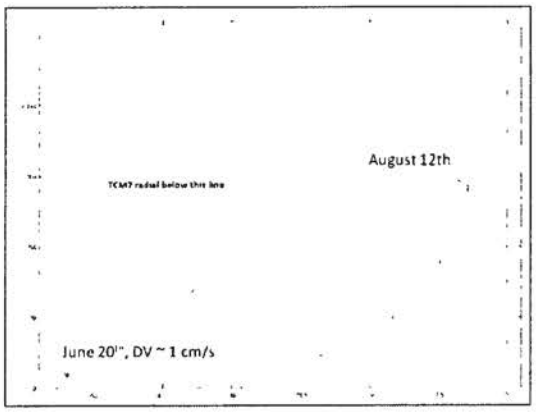


**Figure 11. Analysis of P1 TCM7 Placement**

Upon completion of TCM6, TCM7 and TCM8 corrected performance errors of TCM6 and the final targeting to the libration insertion state and the epoch. The need for TCM8 arises from the planned the EM $L_2$ to the EM $L_1$ transfer Z-component required for the libration orbit portion of the mission. Without TCM8, the transfer trajectory would achieve a polar lunar orbit. With TCM8, a closing $L_2$ orbit with the correct $L_1$ planar orbit was correctly achieved. There are also uncertainties in post TCM7 and TCM8 OD solutions. Late July and later August OD solutions indicate a need for TCM8 to control the Z-evolution of the libration orbit itself. Early August OD solutions indicate no TCM8 required. Investigation into OD solution accuracy and quality led to acceptance of later solutions, confirmed with GSFC's FDF solutions. Variation in stationkeeping Δvs over the duration of EM $L_2$ and EM $L_1$ orbits changed the Z-evolution profile thus required TCM8 for Z-control using the latest OD solutions. The MC analysis for TCM8 is shown in figure 12. The averaged Δv was 0.51 m/s with the max Δv of 2.9 m/s. The standard deviation was 0.623 m/s.

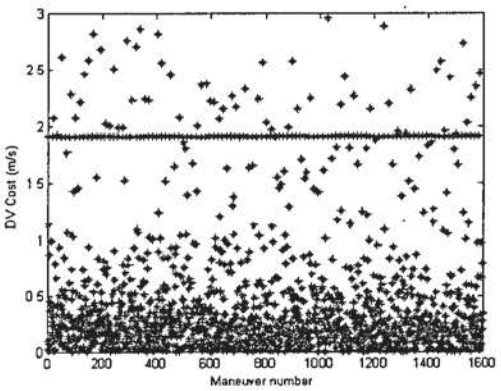


**Figure 12. P1 TCM8 MC Analysis**

The numerically generated trajectories for two maneuvers, the P1 DSM and P1 TCM5, appear in Figures 13 and 14 as they were executed. Note how the resulting (post maneuver) trajectory varied due to maneuver execution and navigation errors as well as any mismodeling in solar radiation pressure. The largest difference is shown in the post-DSM trajectory as the maneuver error was significant at 11 cm/s. In the TCM5 maneuver used to correct the DSM error, the resultant accuracy yielded an error of 0.4 cm/s. This error was corrected in the TCM6 maneuver. Two additional TCM maneuvers were then executed to adjust the arrival epoch into the Earth-Moon entry point and subsequent Lissajous trajectory.

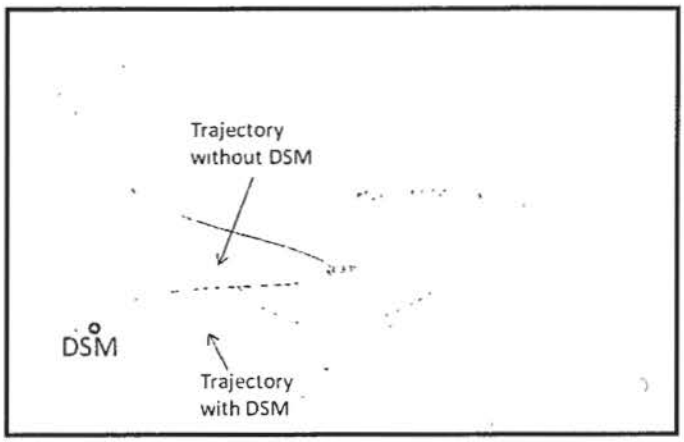


**Figure 13. Preplanning and Optimized P1 DSM**

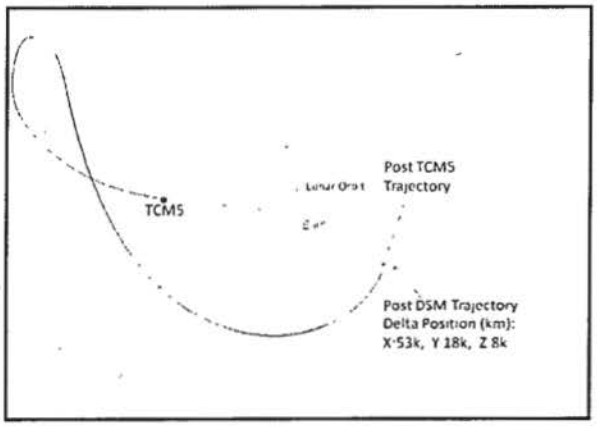


**Figure 14. Optimized TCM5 Trajectory**

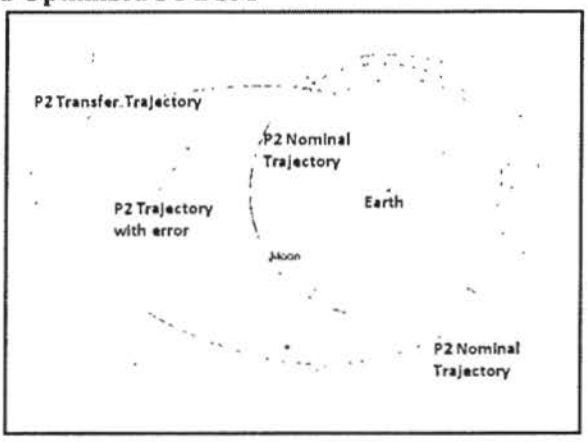


**Figure 15. Post P2 DSM and TCM3 Trajectory**

These time change maneuvers were required to permit the correct $Z$ amplitude-evolution in both the $L_2$ and $L_1$ orbits. Recall that for a Lissajous orbit the $Z$ frequency is not correlated with the in-plane frequency, thus, a change to the Lissajous insertion time provides a method to adjust the initial velocities and Z component amplitudes. Figure 15 presents the P2 trajectory for the optimized DSM and the correction TCM. As is apparent, the trajectory diverges after approximately one revolution around Earth, where the orbit radius is beyond the lunar orbit radius. In contrast, the corrected trajectory passes by the EM $L_2$ side using a half-Lissajous and then transfers to the EM $L_1$ side.

Figure 16 illustrates how P2 was indirectly inserted into the $L_1$ Lissajous orbit. The strategy was to fly past the $L_2$ point, and using the P2's TCM4, TCM5, and lunar gravity to transfer the orbit over to the the $L_1$ orbit. Leveraging the lunar gravity allowed for a low-cost insertion into $L_1$ orbit; a direct insertion into the $L_2$ orbit would have required much higher $\Delta v$. TCM4 and TCM5 were designed as a pair to minimize total $\Delta v$. Figure 17 illustrates the effect of quantization of TCM4 on TCM5. The optimized solution found that a TCM4 of 14 pulses significantly minimized the magnitude of TCM5; A 15-pulse would have increased TCM5 by a factor of three, while a 13-pulse TCM4 would have increased TCM5 by a factor of six. A 14-pulse TCM4 was the best choice, and the operations team adjusted the pre-maneuver calibration to ensure that TCM4 would burn slightly hot, ensuring that the maneuver performance was near the trough in the optimization curve.

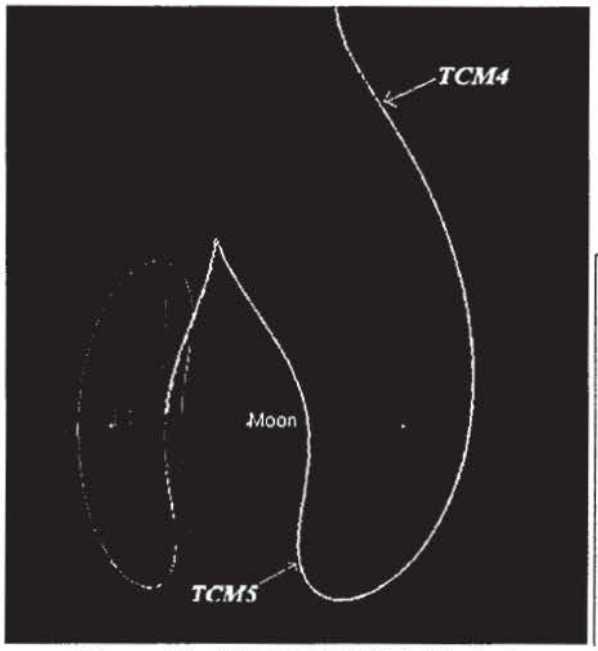


Figure 16. P2 TCM4/TCM5 Trajectory

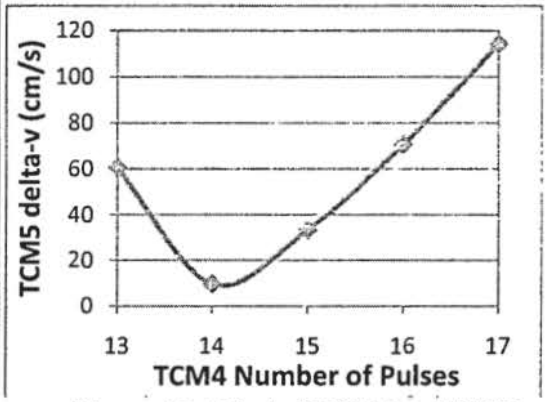


Figure 17. Effect of TCM4 on TCM5

## MULTI-BODY DYNAMICAL ENVIRONMENT MANIFOLDS

A manifold is a representation of local trajectories that are subsequently numerically integrated in a full ephemeris model.[11-16] Additionally, 'manifolds' are frequently represented either by the numerical results, by algorithms that define the state-space via lower-fidelity circular restricted modeling, or even by continuously differentially corrected arcs. The manifolds plotted in this paper are constructed using the initial and ephemeris states of the optimal or actual navigation solutions, meaning they represent a higher-fidelity model of all local (nearby) trajectories.

For ARTEMIS, manifolds that exist in the multi-body dynamical environment were generated to verify the numerically integrated, optimally planned, and actual post-maneuver results. The computation of manifolds also demonstrates the design process that can potentially shift a trajectory arc from the vicinity of one manifold to another and, thus, attain the targeted Lissajous insertion states (that is, an $L_2$ state for the P1 spacecraft and an $L_1$ state for the P2 spacecraft). These manifold computations are used essentially to interpret the effects of the DSM and the TCM maneuvers and to illustrate how the stable or unstable manifolds do, in fact, intersect near the maneuver locations. Manifolds are plotted for the pre- and post-DSM and TCM5 maneuvers of the P1 spacecraft and for the pre- and post-DSM-1 trajectory arcs for the P2 spacecraft. In Figure 18, the P1 stable manifold appears, reflecting the actual trajectory as designed, for the optimal condition that would permit P1 to coast throughout the trajectory to the point of maximum excursion; subsequently, the spacecraft would closely follow the flow consistent with an unstable manifold to eventually arrive at the $L_2$ insertion location. But, as with all maneuvers and operations, errors in maneuver execution and navigation error affect the results. As noted, for the P1 spacecraft, two manifolds are actually used to represent the behavior of the system, i.e., the stable manifold which traverses the outbound trajectory and the unstable manifold which provides a path to deliver the spacecraft to the Earth-Moon Lissajous orbit insertion state. From the DSM, P1 follows the original outbound path to the location of TCM5. Note that TCM 5 shifted the spacecraft to a different path, one that can be envisioned in terms of a different manifold. Subsequent to the DSM, and along the outbound trajectory, two outbound manifold arcs emerge from the TCM5 location and are plotted in Figures 9, 10, and 11.

These two manifolds represent the potential outcomes from (1) flow along the optimal path and (2) the alternative that incorporates a possible TCM5 maneuver. Figure 16 presents the optimal (planned) DSM manifold. Note the location of the potential TCMs in this design. Figure 17 reflects the maneuver effect of an exaggerated TCM5 applied to correct for a DSM execution error and demonstrates the P1 'jump' from the vicinity of one stable manifold (green) to an alternate transfer path that is represented by flow along another manifold (orange). For ARTEMIS, the manifolds were not directly incorporated to determine the optimal maneuver locations but to assess the feasibility and dynamical foundation of the overall structure of the design. Manifold intersections as part of the design process to determine maneuver locations can be done and has been proven both in research and in operations for the Genesis mission.[17,18] The P1 unstable manifold and the effect of TCM5 on the return portion of the orbit are plotted in Figure 19 for an exaggerated TCM5 maneuver. The figure includes the original planned and the corrected post TCM5 trajectory. For the actual, relatively small TCM5 maneuver, the difference is slight in terms of the larger design but the shift in the general direction of the flow is consistent with a new manifold; the post TCM5 path with a small shift in direction guaranteed that P1 would reach its goal at the proper epoch.

The actual path for the P2 spacecraft (blue) as well as a computed manifold surface (green) appears in Figure 21. This manifold design reflects the corrected manifolds to deliver the vehicle directly from the DSM to the vicinity of the Earth-Moon Lissajous stable manifold. Off-nominal conditions require a maneuver that shifts to the vicinity of this same manifold to successfully arrive at the Earth-Moon Lissajous orbit. Similar to the P1 design, the manifold is used to verify the feasibly of the optimized correction maneuver. The P2 spacecraft also jumps or shifts from the vicinity of one manifold to flow in a direction consistent with the required manifold at the maneuver location.

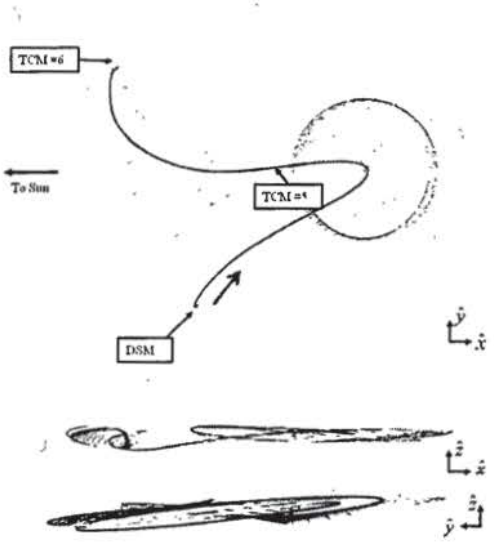


**Figure 18. P1 Planned Stable Sun-Earth Manifold**

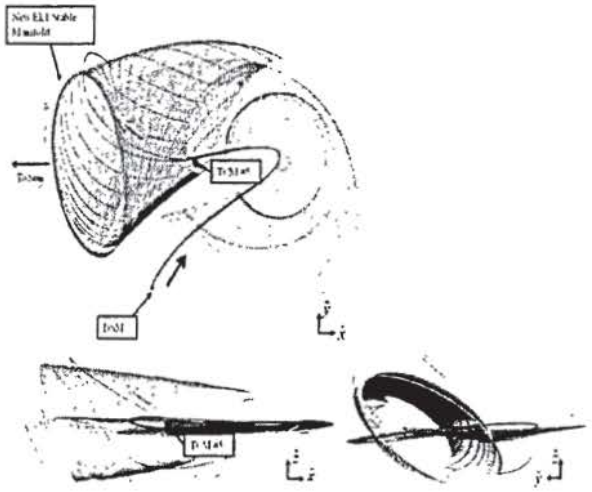


**Figure 19. P1 Pre and Post TCM5 Stable Sun-Earth Manifold**

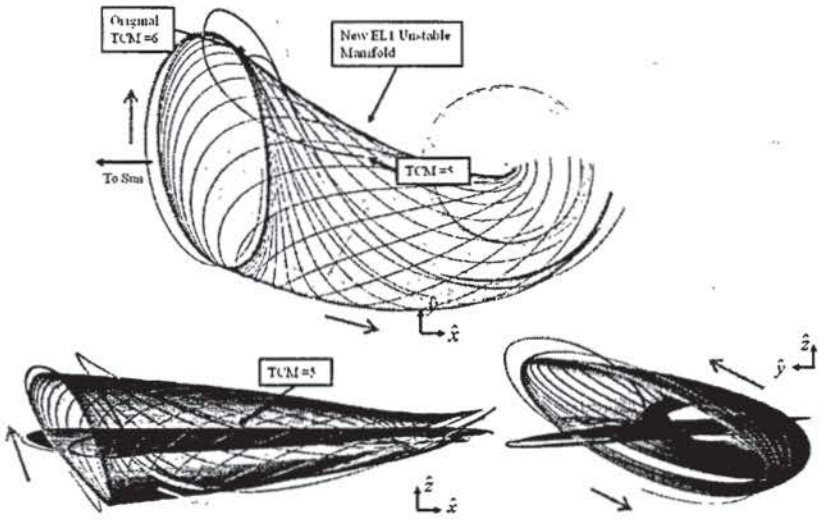


**Figure 20. P1 Post TCM5 Unstable Manifold to $L_2$ Lissajous Targeted State**

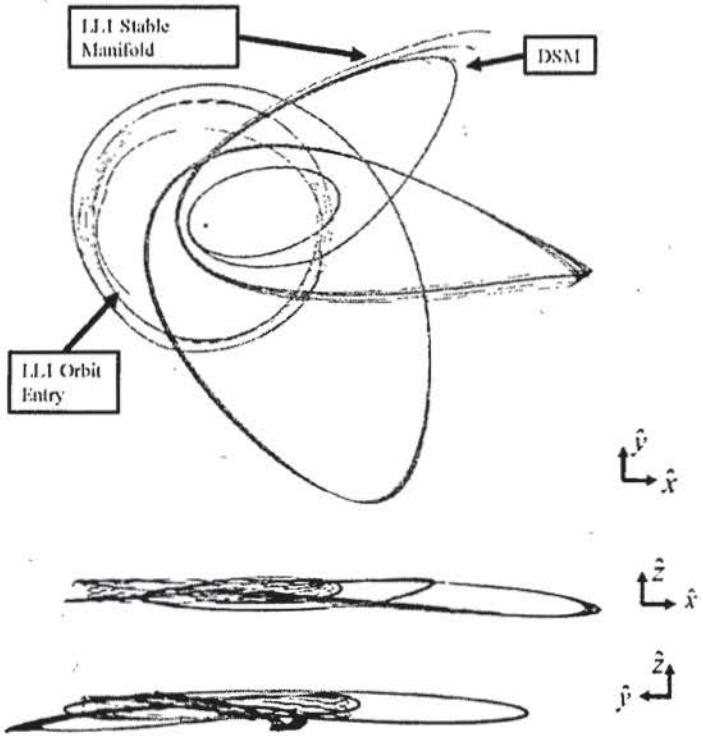


**Figure 21. P2 Manifold to $L_1$ Lissajous Targeted State**

## SUMMARY

The ARTEMIS challenges of the spacecraft constraints, the multi-body dynamical environment, and the navigation performance can be overcome by the judicious use of optimization tools and manifold

generation for verification. Reliable software tools such as GMAT and AGI's STK/Astrogator were available to permit cross checking of all maneuver plans and predicted trajectories. The overall sensitivity of the trajectory to the dynamical environment was found to be near the anticipated levels as those proposed from many theoretical investigations and from recent operational missions that briefly flew trajectories which passed thought these multi-body dynamical environments. Small errors produced a large effect on the transfer design, but small, well-placed maneuvers can also correct these errors. While there are a number of strategies available that incorporate the Earth-Moon dynamics, the actual mission applications and mission constraints must also be considered. The methods developed here allow a general application whether there is a reference orbit, spacecraft constraints on $\Delta v$ direction, or orbital parameters requirements. The required transfer $\Delta v$ budget can be minimized and the capability to reduce the budget to a very low level is substantially enhanced by exploiting the dynamical structure.

## CONCLUSIONS

The ARTEMIS mission is an unqualified success which can be attributed to the use of several tools to validate and confirm the planning and execution of maneuvers necessary to transit a dynamically challenging environment. The combined method of optimization with manifold verification, thought not new, is a substantial leap in the operational design of such missions. With the completion of the ARTEMIS trajectory, a viable multi-tiered process and trajectory feasibility is demonstrated. The opportunities of the ARTEMIS mission provide the space community with the first ever completed design from Earth to the Earth-Moon $L_2$ and $L_1$ Lissajous orbits. Both spacecraft have completed their mutli-body mission in both the transfer and the Earth-Moon libration orbits and are now orbiting in elliptical lunar orbits.

## ACKNOWLEDGEMENTS

The authors would like to acknowledge Manfred Bester, Sabine Frey, Jeff Marchase, Brandon Owens and Swapan Gandhi at the University of California Berkeley Space Science Laboratory. Their operational expertise and open communications ensured a successful mission. We also would like to thank Tom Pavlak and Dr. Howell of Purdue University for their support in the generation of manifolds and answering the many related questions.

## REFERENCES

1. V. Angelopoulos and D. G. Sibeck, "THEMIS and ARTEMIS," a proposal submitted for the Senior Review 2008 of the Mission Operations and Data Analysis Program for the Heliophysics Operating Missions; available at http://www.igpp.ucla.edu/public/THEMIS/SCI/Pubs/Proposals%20and%20Reports/-HP SR 2008 THEMIS SciTech 20080221.pdf, 2005.

2. Folta, D. Sweetser, T., " ARTEMIS Mission Overview, From Concept to Operations", AAS/AIAA Astrodynamics Specialist Conference held August 1-4 2011,Girdwood, Alaska.

3. Woodard, M., Folta, D., and Woodfork, D., "ARTEMIS: The First Mission to the Lunar Libration Points," 21st International Symposium on Space Flight Dynamics, Toulouse, France September 28-October 2, 2009.

4. Broschart S., et al, "Preliminary Trajectory Design for the Artemis Lunar Mission", AAS 09-382, AAS/AIAA AstrodynamicsSpecialist Conference held August 9-13 2009, Pittsburgh, Pennsylvania.

5. Folta, D., Howell, K., "Application of Multi-Body Dynamical Environments: The ARTEMIS Transfer Trajectory design", 61st International Astronautical Congress, Prague, Czech Republic.

6. Gómez, G., Llibre, J., Martínez, R., and Simó, C., *Dynamics and Mission Design Near Libration Points, Vol. I: Fundamentals: The Case of Collinear Libration Points*, World Scientific Monograph Series, World Scientific Publishing Ltd., Singapore, 2001.

7. Howell, K.C., and Marchand. B.G., "Natural and Non-Natural Spacecraft Formations Near the $L_1$ and $L_2$ Libration Points in the Sun-Earth/Moon Ephemeris System," *Dynamical Systems: an International Journal,* Special Issue: "Dynamical Systems in Dynamical Astronomy and Space Mission Design," Vol. 20, No. 1, March 2005, pp. 149-173.

8. W. S. Koon, M. W. Lo, J. E. Marsden, and S. D. Ross, "Heteroclinic Connections Between Periodic Orbits and Resonance Transitions in Celestial Mechanics," Chaos, Vol. 10, No. 2, 2000, pp. 427–469.

9. Gómez, G., Jorba, A., Masdemont, J., and Simó, C., "Study of the Transfer from the Earth to a Halo Orbit Around the Equilibrium Point $L_1$," *Celestial Mechanics and Dynamical Astronomy*, Vol. 56, No. 4, 1993, pp. 541-562.

10. Howell, K.C., Mains, D.L., and Barden, B.T., "Transfer Trajectories from Earth Parking Orbits to Sun-Earth Halo Orbits," *AAS/AIAA Space Flight Mechanics Meeting 1994*, Advances in the Astronautical Sciences, Vol. 87, J. Cochran, C. Edwards, S. Hoffman, and R. Holdaway (editors), 1994, pp. 399-422.

11. Barden, B.T., and Howell, K.C., "Fundamental Motions Near Collinear Libration Points and Their Transitions," *Journal of the Astronautical Sciences*, Vol. 46, No. 4, October-December 1998, pp. 361-378.

12. Belbruno, E.A., "Sun-perturbed Earth-to-Moon Transfers with Ballistic Capture. Journal of Guidance Control and Dynamics, 16(4): 770-775, 1993

13. Belbruno, E.A., "The Dynamical Mechanism of Ballistic lunar Capture Transfers in the Four Body Problem from the Perspective of Invariant manifolds and Hill's Regions", Institut D'Estudis Catalans CRM Research Report No.270.

14. Bello-Mora, M. F., Graziana P. T., et al, "A systematic Analysis on Weak Stability Boundary Transfers to the Moon. *In* Proc 51st International Astronautical Congress IAF-00-A.6.03, Rio de Janeiro, Brazil. 2000

15. Howell, K.C., Barden, B.T., and Lo, M.W., "Application of Dynamical Systems Theory to Trajectory Design for a Libration Point Mission," *Journal of the Astronautical Sciences*, Vol. 45, No. 2, April-June 1997, pp. 161-178.

16. Barden, B.T., Wilson, R.S., Howell, K.C., and Marchand, B.G., "Summer Launch Options for the Genesis Mission," AAS/AIAA Astrodynamics Specialists Conference, Quebec City, Canada, July 30 - August 2, 2001.

17. Whiffen, G.J., "Mystic: Implementation of the Static Dynamics Optimal Algorithm for High Fidelity Low Thrust Trajectory Design" Proceedings of the AIAA/AAS Astrodynamics Specialists Conference, Keystone, CO, 2006, Paper AIAA 2006-6741